PNAS RESEARCH ARTICLE | PHYSICS

Photoelectron spectroscopy with entangled photons; enhanced spectrotemporal resolution

Bing Gu[a,b,1], Shichao Sun[c,d], Feng Chen[c,d], and Shaul Mukamel[c,d,1]

Contributed by Shaul Mukamel; received January 11, 2023; accepted April 3, 2023; reviewed by Anna I. Krylov and Hans Jakob Wörner

In this theoretical study, we show how photoelectron signals generated by time-energy entangled photon pairs can monitor ultrafast excited state dynamics of molecules with high joint spectral and temporal resolutions, not limited by the Fourier uncertainty of classical light. This technique scales linearly, rather than quadratically, with the pump intensity, allowing the study of fragile biological samples with low photon fluxes. Since the spectral resolution is achieved by electron detection and the temporal resolution by a variable phase delay, this technique does not require scanning the pump frequency and the entanglement times, which significantly simplifies the experimental setup, making it feasible with current instrumentation. Application is made to the photodissociation dynamics of pyrrole calculated by exact nonadiabatic wave packet simulations in a reduced two nuclear coordinate space. This study demonstrates the unique advantages of ultrafast quantum light spectroscopy.

entangled light | photoelectron spectroscopy | photodissociation

Significance

Quantum light sources bring unique opportunities for nonlinear spectroscopy resulting in quantum spectroscopy with no classical analogs and enhancing the sensitivity and resolution of classical spectroscopy. Here, we present a photoelectron signal obtained by a time-frequency entangled photon pair with high spectral and temporal resolution owing to the time and frequency correlation of the twin photons. This is not possible for classical light due to the fundamental Fourier uncertainty. Furthermore, we demonstrate that the signal scales linearly, rather than quadratically, with the pump intensity, allowing the study of delicate samples at low photon flux. This technique does not require scanning the pump frequency and entanglement times and is experimentally feasible with current instrumentation.

Nonlinear spectroscopy has been instrumental for probing dynamical processes in a wide variety of material systems ranging from atoms, molecules to biological complexes and semiconductors (1–3). These techniques mostly rely on coherent laser pulses with well-defined electric field and phase. Employing quantum light in nonlinear molecular spectroscopy has brought many novel opportunities to enhance the signal-to-noise ratio, the resolution, and the selectivity of transition pathways (4–15).

Photon entanglement offers a new and unique spectroscopic knob that is not available by classical laser pulses. One notable example is entangled two-photon absorption technique (ETPA, i.e., two-photon absorption with entangled photon pairs), which has attracted much recent interest (16–21). ETPA differs from classical two-photon absorption in many ways. First, the absorption cross-section scales linearly, rather than quadratically, with the pump intensity (22), reducing the risk of photodamage of fragile samples. Enhancement magnitude of ETPA over classical light with the same photon flux is under current (10) experimental and theoretical studies' debate (21, 23, 24). Additional intricate features associated with entangled photons have been proposed. For example, it was shown that entangled photons can probe classically forbidden transitions. These states are dark in classical two-photon absorption due to destructive interference. This interference can be controlled and eliminated by entangled photons (20). Another example is entangled photon-pair two-dimensional fluorescence spectroscopy (17), which employs the Franson interferometer (25). In a recent theoretical study, ETPA has been used to monitor conical intersection dynamics in molecules in real time by employing further time delays (26). It was further theoretically suggested that Raman scattering can be enhanced by positive frequency correlations of entangled photons (27).

Quantum interferometers such as Hong-Ou-Mandel (28) and coincidence detection are being explored for spectroscopic applications (29–33). With molecules inserted in one possible photon pathway, information is revealed by how the presence of matter affects the interference pattern. Because such interferometers typically operate at the few-photon level, quantum interferomertic spectroscopy has no analogs with coherent classical light source. Theoretical studies have shown that such setups can be used to select Liouville space pathways that cannot be achieved with classical light, and measure correlation functions that do not arise in the optical response to classical stimulus (29).

Quantum light spectroscopy shows great promise for extracting new information of matter by novel spectroscopic techniques and measurements, which have no classical analogues.

In this theoretical study, we propose a time-resolved entangled photoelectron spectroscopy (EPES) technique, which employs a time-frequency entangled photon pair, and demonstrate how it can be used to monitor the photodissociation dynamics

Author contributions: B.G., F.C., and S.M. designed research; B.G., S.S., F.C., and S.M. performed research; and B.G. and S.M. wrote the paper.

Reviewers: A.I.K., University of Southern California; and H.J.W., Swiss Federal Institute of Technology in Zurich.

The authors declare no competing interest.

[1]To whom correspondence may be addressed. Email: gubing@westlake.edu.cn or smukamel@uci.edu.

This article contains supporting information online at http://www.pnas.org/lookup/suppl/doi:10.1073/pnas.2300541120/-/DCSupplemental.

Published May 15, 2023.

of the pyyrole molecule, schematically shown in Fig. 1. A narrowband pump beam passing through a nonlinear crystal creates entangled photon pairs, historically known as signal and idler, by a spontaneous parametric down-conversion (SPDC) process. The signal photon first brings the molecule into an electronically excited state, initiating the photochemical process. The idler photon, time-delayed by a phase shifter, then interrogates the molecule by ionization. The signal-idler time delay is scanned and the energy-resolved photoelectron is detected. We demonstrate that this technique allows virtually unlimited joint spectral and temporal resolution, which is not possible with classical light. In time-resolved photoelectron spectroscopy with classical ultrashort pulses, the temporal and spectral resolutions are subjected to the Fourier uncertainty, $\sigma_{\omega+\omega'}\sigma_{t-t'} \geq 1$ where σ denotes standard deviation. Broadband pulses must be used to achieve the temporal resolution at the expense of spectral resolution. Frequency resolution can be improved by narrowband pulses, which however erodes the time resolution. For entangled photons, while both photons can be broadband, the sum of their frequencies can be very narrowly distributed when a narrowband pump pulse is used in the SPDC process. In classical photoelectron spectroscopy, an ultrashort laser pulse is used to launch the photoreaction, thus we know precisely when the molecule is photoexcited. In EPES, the arrival time of the signal photon is random with uncertainty determined by the pump bandwidth. However, the arrival time difference between signal and idler, $t_s - t_i$, is determined by the entanglement time, which can be made very short by using a thin crystal. This is because for entangled photons, $t_s - t_i$ is not the Fourier conjugate of the sum frequency $\omega_s + \omega_i$.

Moreover, the linear rather than quadratic scaling of the EPES signal with the pump intensity allows the study of fragile samples with low photon flux. This advantage is shared by ETPA, and comes from the bunching of the twin photons, rather than from the entanglement (34). Furthermore, the spectral resolution is achieved by energy-resolved electron detection and the temporal resolution is independently determined by a variable phase delay, Thus, it is not necessary to scan the pump frequency and the entanglement time, which greatly simplifies the experimental setup making it feasible with current instrumentation.

We apply EPES to study the photodissociation dynamics of pyrrole molecule which involves a passage through a conical intersection. The exact nonadiabatic wave packet dynamics is calculated for a vibronic model (35) that includes two nuclear degrees of freedom. Pyrrole is a prototypical heteroaromatic molecule with vanishingly small fluorescence quantum yield due to nonradiative decay channels between the excited and the ground electronic states. The photoelectron spectroscopy of pyrrole has been measured previously using classical femtosecond lasers with broad kinetic energy distribution of photoelectrons (36). We demonstrate how entangled photons can monitor the nonadiabatic dynamics in real time and resolve the final dissociation channels, which is not possible with classical light. Our results clearly demonstrate the merits of employing quantum light for monitoring ultrafast molecular dynamics in real time.

Atomic units $m_e = e = \hbar = 1$ are used throughout.

Theory. The total Hamiltonian $H = H_M + H_R + H_{RM}$ consists of the molecular Hamiltonian H_M representing the electron-nuclear motion, the quantized radiation Hamiltonian H_R describing the entangled light. The interaction between the entangled photon pair and molecules in the electric dipole gauge and the rotating-wave approximation reads

$$H_{RM} = -\mathbf{V}^\dagger \cdot \left(\hat{\mathbf{E}}_s^{(+)} + \hat{\mathbf{E}}_i^{(+)}\right) + \text{H.c.}, \qquad [1]$$

where $\hat{\mathbf{E}}_{s/i}^{(+)} = \mathbf{e}_{s/i}\hat{E}_{s/i}$ is the (transversal) electric field operator of signal/idler photon beam (37) and $\mathbf{V}$ ($\mathbf{V}^\dagger$) is the lowering (raising) component of the dipole operator, $\boldsymbol{\mu} = \mathbf{V} + \mathbf{V}^\dagger$, and H.c. stands for Hermitian conjugate.

The EPES signal is given by the time-averaged electron flux with momentum $\mathbf{k}$

$$S(\mathbf{k}) = \int_{-\infty}^{+\infty} d\mathbf{t} \mathrm{Tr}\{\dot{\mathbf{N}}_{\mathbf{k},H}(\mathbf{t})\rho_0\} \qquad [2]$$

where $N_{\mathbf{k}} = \hat{\phi}_{\mathbf{k}}^\dagger \hat{\phi}_{\mathbf{k}}$ is the electron number operator of momentum $\mathbf{k}$ with annihilation (creation) operator $\hat{\phi}_{\mathbf{k}}$ ($\hat{\phi}_{\mathbf{k}}^\dagger$), and ρ_0 is the initial total density matrix. The subscript H denotes the Heisenberg picture. Using fourth-order time-dependent perturbation theory in H_{RM}, the signal can be read off the loop diagram in Fig. 2

$$S(\mathbf{k}) = \int_{t_0}^{\infty} dt_2 \int_{t_0}^{t_2} dt_1 \int_{t_0}^{\infty} dt_2' \int_{t_0}^{t_2'} dt_1' \langle \Psi_I | V_s(t_1') V_i(t_2') N_{\mathbf{k}} V_i^\dagger(t_2) V_s^\dagger(t_1) | \Psi_I \rangle G(t_1', t_2', t_2, t_1), \qquad [3]$$

where $G(t_1', t_2', t_2, t_1) = \langle \Phi | \hat{E}_s^{(-)}(t_1') \hat{E}_i^{(-)}(t_2') \hat{E}_i^{(+)}(t_2) \hat{E}_s^{(+)}(t_1) | \Phi \rangle$ is a field correlation function, and $O(t)$ denotes the operator O in the interaction picture with the noninteracting

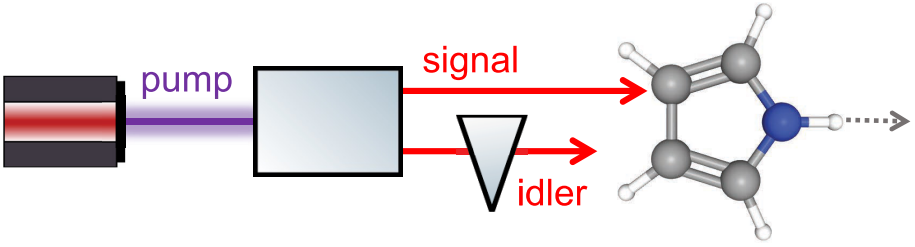

Fig. 1. The entangled photoelectron spectroscopy setup. A narrowband pump pulse impinges a nonlinear crystal to create an entangled photon pair, signal and idler. The signal photon excites the molecule, triggering a photochemical reaction. The time-delayed idler photon finally interrogates the molecule by photoionization. The ejected photoelectron is detected.

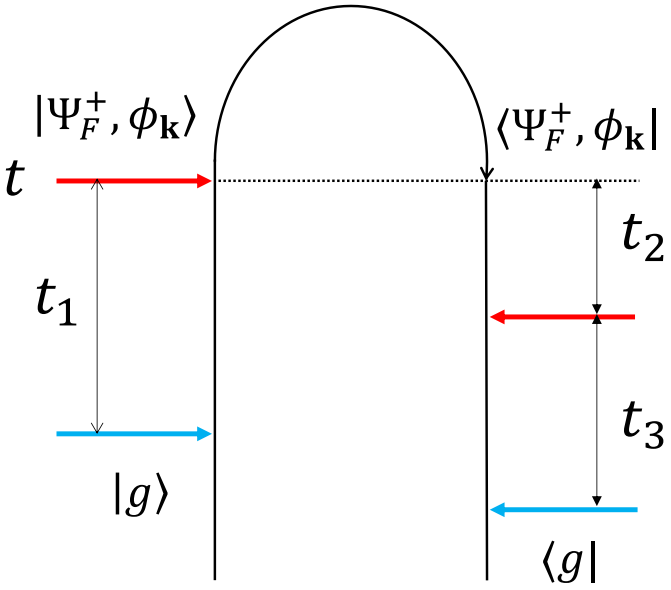

Fig. 2. Time-loop diagram for the time-resolved entangled photoelectron spectroscopy. Blue/red arrows indicate interaction with signal/idler photon. $t_i \in (0, \infty)$ are time intervals between light–matter interactions in the time-dependent perturbative expansion that are integrated to yield the final signal. The rules for the time-loop diagrams can be found in ref. 38.

Hamiltonian of matter and field $H_0 = H_\mathrm{M} + H_\mathrm{R}$. Here $|\Psi_I\rangle$ is the initial electron-vibrational (vibronic) state, $|\Phi\rangle$ is the twin-photon state.

When the two-photon and the molecule are in a pure state, the photon correlation function can be factored out and **3** simplifies to $S(\mathbf{k}) = \sum_F |\mathbf{T}_{FI}|^2$, with the transition amplitude given by

$$T_{FI} = \int_{t_0}^{\infty} \mathrm{d}t_2 \int_{t_0}^{t_2} \mathrm{d}t_1 \, \langle \Psi_F^+ \mathbf{k}| \, V_\mathrm{i}^\dagger(t_2) V_\mathrm{s}^\dagger(t_1) |\Psi_I\rangle A(t_2, t_1), \quad [4]$$

where $A(t_2, t_1) = \langle 0|\hat{E}_\mathrm{i}(t_2)\hat{E}_\mathrm{s}(t_1)|\Phi\rangle$ is the two-photon amplitude and $|0\rangle$ denotes the vacuum state, $|\Psi_F^+\rangle = |\psi_f, \chi_{\nu_f}\rangle$ is the final vibronic eigenstate of the cation molecule with energy E_F, $F = (f, \nu_f)$ is a composite index indicating vibrational state ν_f on the fth adiabatic potential energy surface.

The Time-Frequency Entangled Photon Pairs. We consider entangled photons created by a type-II SPDC process whereby a pump photon splits into a pair of entangled twin-photons by interaction with a second-order nonlinear crystal. The twin-photon frequencies are anticorrelated due to energy conservation. The two-mode squeezed state of the twin-photons reads

$$|\Phi\rangle = \iint \mathrm{d}\omega_\mathrm{s} \mathrm{d}\omega_\mathrm{i} J(\omega_\mathrm{s}, \omega_\mathrm{i}) a_\mathrm{s}^\dagger(\omega_\mathrm{s}) a_\mathrm{i}^\dagger(\omega_\mathrm{i})|0\rangle, \quad [5]$$

where $J(\omega_1, \omega_2)$ is the (unnormalized) joint spectral amplitude characterizing the joint probability amplitude of the signal photon at frequency ω_s and idler photon at ω_i.

The creation of entangled photons is calculated perturbatively (39, 40). Thus, the twin-photon flux depends linearly on the pump electric field. For a monochromatic pump with frequency ω_p , we have (*SI Appendix*, section S2 for the derivation)

$$J(\omega_\mathrm{s}, \omega_\mathrm{i}) \propto E_\mathrm{p} \delta(\omega_\mathrm{p} - \omega_\mathrm{s} - \omega_\mathrm{i}) \mathrm{sinc}\left(\frac{\Delta\omega_\mathrm{s} T_\mathrm{e}}{2}\right), \quad [6]$$

where the entanglement time T_e characterizes the maximum time delay between signal and idler photons, and $\Delta\omega_\mathrm{s} = \omega_\mathrm{s} - \Omega_\mathrm{s}$ is the detuning from the central frequency Ω_s, and E_p is the electric field amplitude of the pump beam. The Dirac delta function ensures energy conservation, and the sinc function arises from the momentum phase matching condition.

Fourier transforming the joint spectral amplitude to the time domain taking into account the signal-idler time delay T controlled by an optical delay line, and inserting it in Eq. **3** leads to the final expression for the signal (*SI Appendix*, section S2)

$$S(\omega_\mathrm{p}, T) \propto I_\mathrm{p} \sum_F \delta(\omega_\mathrm{p} - E_F - E_\mathbf{k}) \times \left| \int_{T - T_\mathrm{e}/2}^{T + T_\mathrm{e}/2} \mathrm{d}\tau \langle \Psi_F^+ \mathbf{k}| \mathbf{V}_\mathrm{i}^\dagger \mathrm{U}_\mathrm{M}(\tau) \mathbf{V}_\mathrm{s}^\dagger |\Psi_I\rangle \right|^2, \quad [7]$$

where $U_\mathrm{M}(t) = e^{-iH_\mathrm{M}t}$ is the molecular propagator, and $|\Psi_F^+\rangle = |\psi_f^+, \chi_{\nu_f}\rangle$ refers to the final cation vibronic state with electronic state $|\psi_f\rangle$ and vibrational state $|\chi_{\nu_f}\rangle$, $|\Psi_I\rangle = |\psi_0, \chi_0\rangle$ the initial vibronic state, I_p is the pump beam intensity, and $E_\mathbf{k} = \frac{1}{2}|\mathbf{k}|^2$ is the free electron energy. (**7**) implies that the signal scales linearly with the pump intensity, reflecting the non-Poisson statistics of the twin photons. The Dirac delta function ensuring energy conversation reflects the energy anticorrelation of the twin photons. Upon detection of the outgoing electron, the cation energy, and thus state, is fixed by energy conservation. Moreover, the entangled light offers a time window $[T - T_\mathrm{e}/2, T + T_\mathrm{e}/2]$ for interrogating the photodynamics. For short entanglement times, this window is temporally narrow and the signal at time delay T reflects the molecular state at that time. Longer entanglement times will deteriorate the temporal resolution, set by the entanglement time. By exploiting the time-energy entanglement, the EPES signal shows a high temporal and spectral resolution.

Comparison with Classical Photoelectron Spectroscopy (CPES). We now compare the EPES signal with a time-resolved photoelectron signal obtained with two classical ultrashort laser pulses with electric field $E_j(t)$. To achieve similar temporal resolution to EPES, the pump and probe pulses are both broadband. For comparison, we use two coherent pulsed lasers with different bandwidths. The transition amplitude now reads (cf. Eq. **4**)

$$T_{FI}^{(\mathrm{cl})} = \int_{t_0}^{\infty} \mathrm{d}t_2 \int_{t_0}^{t_2} \mathrm{d}t_1 \langle \Psi_F^+ \mathbf{k}| \mathbf{V}_\mathrm{i}^\dagger(\mathbf{t}_2) \mathbf{V}_\mathrm{s}^\dagger(\mathbf{t}_1)|\Psi_I\rangle E_\mathrm{i}^{(+)}(t_2) E_\mathrm{s}^{(+)}(t_1). \quad [8]$$

In contrast to quantum light, there is no delta function that selects a particular final state. With broadband pulses (for good temporal resolution), when the photoelectron is detected, the cation is in a superposition of all final states accessible by the spectral bandwidths of the pump and probe pulses need to be included. For narrowband pulses, it is possible to resolve the final cation state at the expense of the temporal resolution.

EPES and CPES of Pyrrole Photodissociation

We now apply EPES to monitor the NH bond breaking in the photoexcited pyrrole molecule. We have employed the vibronic model Hamiltonian developed in ref. 35. It contains two nuclear

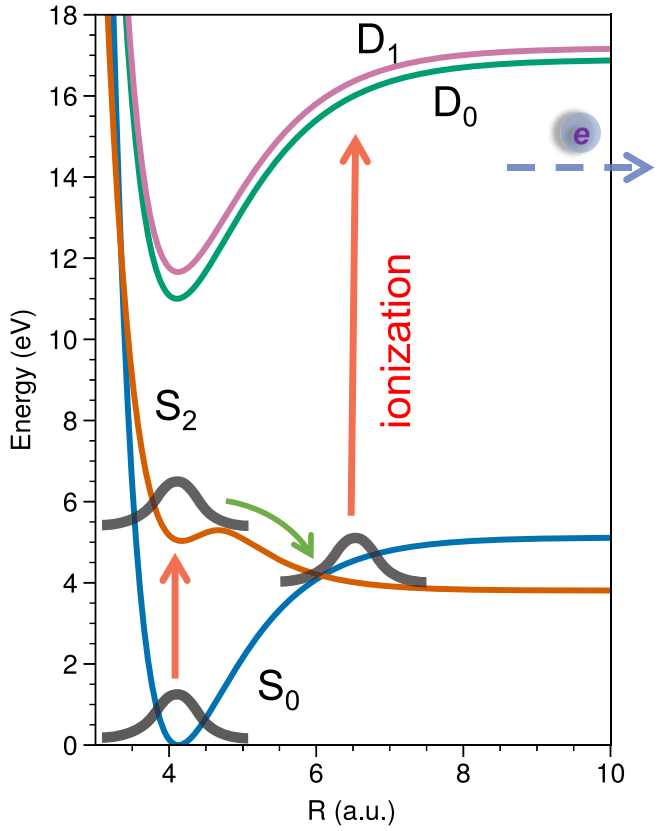

Fig. 3. The neutral and cation potential energy surfaces of pyrrole. Upon photoexcitation to the bright S_2 surface by the signal photon, the nuclear wave packet departs the Franck–Condon region and moves along the slope of surface. It traverses a conical intersection between S_2 and S_0, relaxing nonradiatively to the ground state. *R* is the distance between H and the center-of-mass of the ring.

coordinates, the distance between H and center-of-mass of the ring R and the out-of-plane bending angle θ of the H atom, and two electronic states S_2 and S_0. Slices of the relevant potential energy surfaces along the bond stretching at $\theta = 0$ are shown in Fig. 3. A conical intersection occurs around $r_{NH} = 4.2$ a.u.. The Jacobi coordinates are used for the nuclear kinetic energy operator (35). We have further computed two ionized potential energy surface D_0 and D_1 at the CASSCF level (41, 42). The Dyson orbitals from $S_{0/1}$ to $D_{0/1}$ required to describe the photoelectron signal are calculated at the CASSCF level and depicted in *SI Appendix*, Fig. S1. *SI Appendix*, section S3 for computational details. The potential energy surfaces are scanned along the two nuclear coordinates followed by a least-squares fitting to a functional form shown in *SI Appendix*, section S3. The vibrational eigenstates for the neutral molecule ground state and for the two cation states are calculated by the discrete variable representation (43). The former is required for the initial wave packet, and the latter for determining the final ionized states.

In EPES, the early arriving signal photon brings the oriented pyrrole molecule from the ground electronic state to the bright S_2 state, initiating the N-H bond breaking. For a short entanglement time, the idler photon arrives after a variable time delay T to ionize the molecule. The emitted photoelectron is entangled with the cation, a detection of the electron energy then collapses the cation to a particular energy eigenstate.

The relevant molecular correlation function [**3**] was computed by solving the time-dependent Schrödinger equation for the vibronic model, $i\partial_t \chi_\alpha(\mathbf{R},\mathbf{t}) = \mathrm{K}\chi_\alpha(\mathbf{R},\mathbf{t}) + \sum_\beta \mathrm{V}_{\alpha\beta}(\mathbf{R})\chi_\beta(\mathbf{R},\mathbf{t})$, where K is the nuclear kinetic energy operator and V is the potential energy operator in the diabatic representation. The nuclear wave packets on S_0 and S_2 are calculated on a two-dimensional grid and propagated with the split-operator method (44), *SI Appendix*, section S3 for details of the nonadiabatic wave packet dynamics.

Fig. 4 clearly shows how the nuclear wavepacket, departing from the Franck–Condon region in the excited state, and travels along the surface. Significant population transfer occurs at around 10 fs where the nuclear wavepacket traverses through the conical intersection. Thus, dissociation occurs on both surfaces.

Fig. 5 shows the EPES signal for the conical intersection dynamics vs. the kinetic energy of the photoelectron and signal-idler delay T. Each final cation vibronic state is resolved, generating a narrow line in the spectrum. Initially, there is a strong peak at $E_k = 0.68$ eV, arising from the $S_2(1,0) \rightarrow D_0(1,0)$ ionization channel where (1,0) refers, respectively, to the vibrational quantum number of the stretching mode and bending mode. Although the two modes are not separable, this description is a good approximation for low vibrational states. This peak decays within 5 fs as the nuclear wave packet moves out of the Franck–Condon region. Around 10 fs, there is significant population transfer to the electronic ground state, and ionization due to $S_0 \rightarrow D_1$ start to emerge. This leads to the rise of other dissociation channels, Fig. 5*B*. Some cation eigenstates important for the final photoionization are shown in *SI Appendix*, Fig. S3.

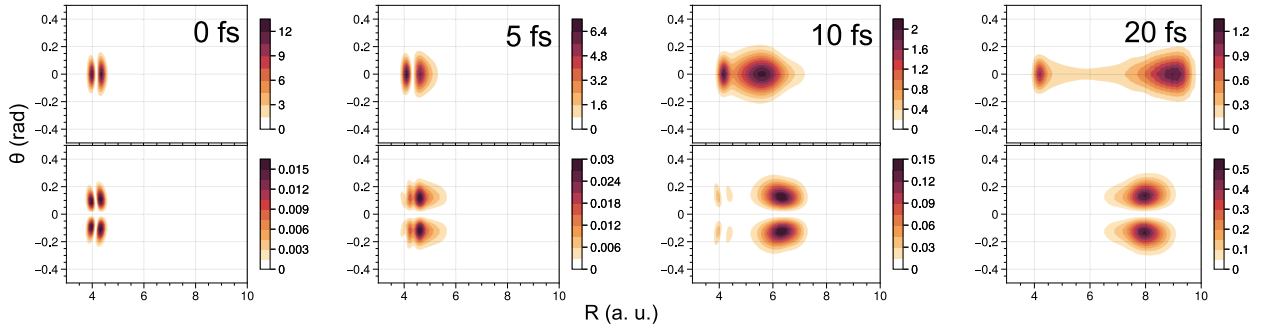

Fig. 4. Nonadiabatic wave packet dynamics of the photodissociation of pyrrole. *Top* panels show the nuclear wavepacket in the excited state potential energy surface S_2, *Bottom* panels correspond to the ground state S_0. Significant population transfer occurs at around 10 fs where the nuclear wavepacket traverses through the conical intersection. Thus, dissociation occurs on both channels.

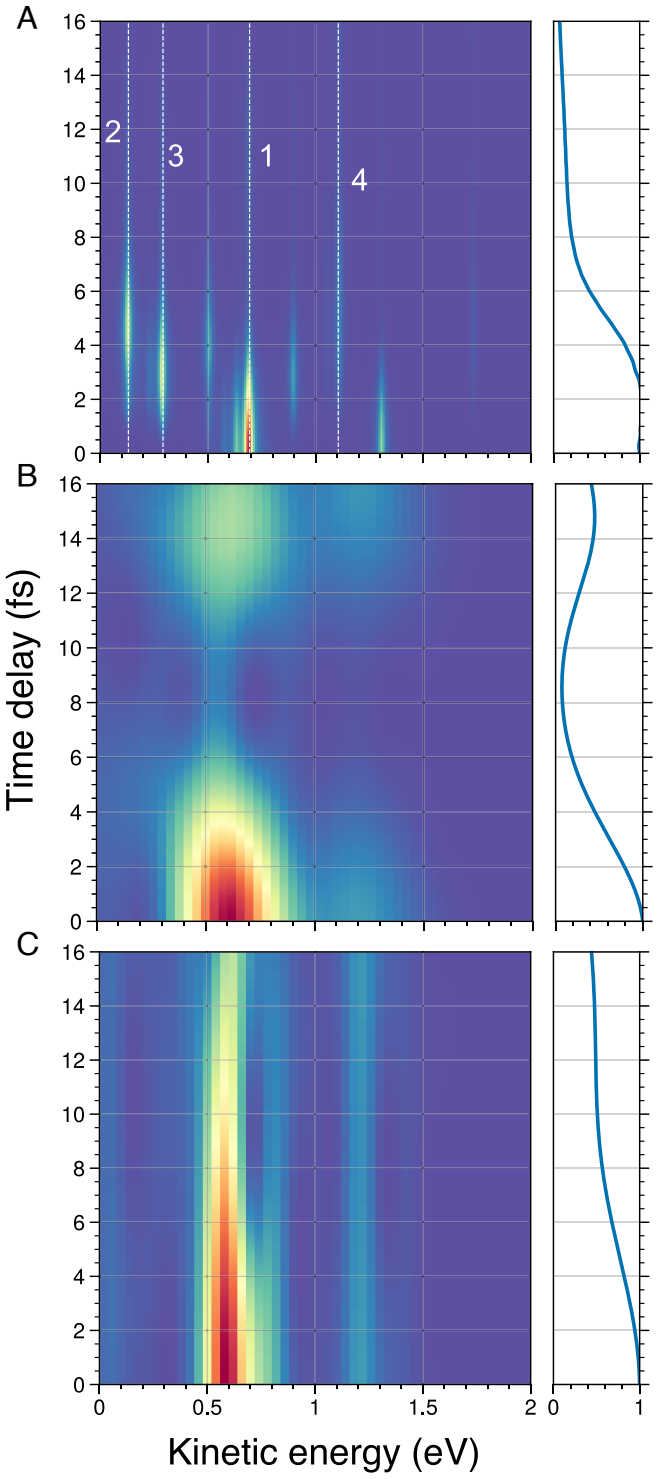

Fig. 5. Comparison of (*A*) the EPES and (*B* and *C*) CPES. The right panels show the frequency-integrated signal, that reflects the electronic relaxation dynamics. The time-resolved CPES with a short pulse (*B*) reveals a good temporal resolution but poor spectral resolution, whereas (*C*) a longer pulse shows a better spectral resolution but poor temporal resolution.

For comparison, we have simulated the CPES spectra with two Gaussian pulses. For pulse duration $\tau = 4$fs, the spectrum exhibits good temporal but poor spectral resolution, which only reveals two broadened features at $\omega_{\mathbf{k}} \sim 0.6, 1.2$ eV (Fig. 5*B*). With a longer pulse $\tau = 8$ fs (Fig. 5*C*), the spectral resolution is improved. Nevertheless, the signal along the time delay deviates significantly from the shorter pulse case, and thus does not reflect the real-time dynamics of the molecule. The contribution of each final ion state to the total signal can be seen by the vertical cuts of the EPES (Fig. 6).

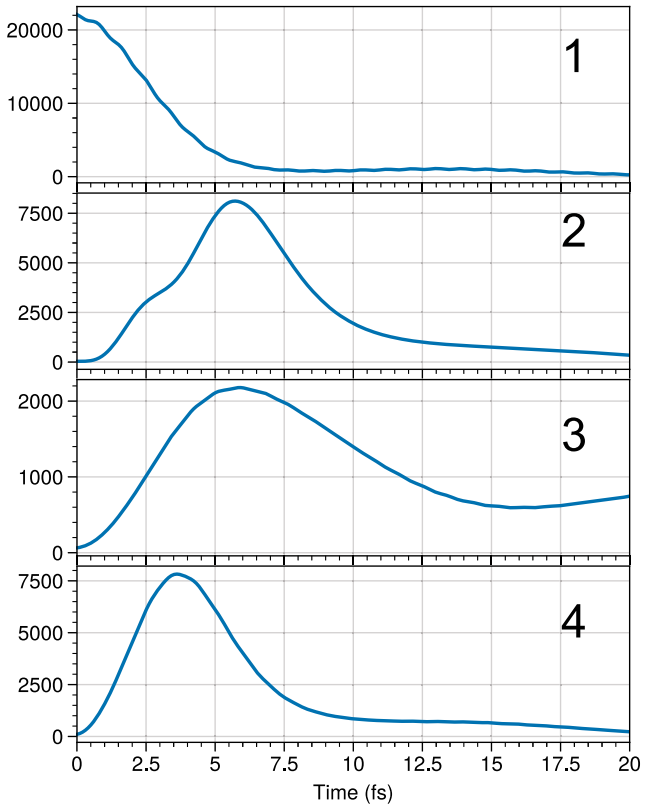

Fig. 6. Vertical cuts of the EPES in Fig. 5*A* showing the temporal resolution.

Conclusions

We have computed the EPES signal with a time correlated and frequency anticorrelated photon pair. Application for the pyrrole photodissociation demonstrated that entangled photons generate very high spectral and temporal resolution not possible with classical light due to the Fourier uncertainty. In EPES, although the arrival of each photon has a large uncertainty, the time difference between signal and idler photons can be precisely controlled by the short entanglement time. Another advantage is that, similar to the entangled two-photon absorption, the EPES technique scales linearly rather than quadratically on the pump intensity, allowing the study of fragile samples at low photon flux. Furthermore, this technique does not require scanning the pump frequency and entanglement times thus simplifying significantly the experimental setup and thus makes it experimentally feasible since the photoelectrons rather than the photons are being detected.

Our results show the great potential of quantum light for monitoring ultrafast dynamical processes in real time. Future directions involve modeling molecules with all vibrational degrees of freedom and studying molecules in a condensed phase environment where bath-induced dephasing must be taken into account.

Supporting Information Appendix (SI). Theory of the twin-photon state; Derivation of Eq. **3**; Computational details for the

nonadiabatic nuclear wavepacket dynamics, electronic structure, and signal calculations.

Data, Materials, and Software Availability. All study data are included in the article and/or *SI Appendix*.

ACKNOWLEDGMENTS. The work was primarily supported by the Chemical Sciences, Geosciences, and Biosciences Division, Office of Basic Energy Sciences, Office of Science, US Department of Energy through Award DE-FG02-04ER15571 (S.S. and F.C.). The support of the NSF Grant No. CHE-2246379 is gratefully acknowledged. S.M. is a fellow of the Hagler Institute for Advanced Study at Texas A&M University.

Author affiliations: [a]Department of Chemistry, School of Science, Westlake University, Hangzhou, Zhejiang 310030, China; [b]Institute of Natural Sciences, Westlake Institute for Advanced Study, Hangzhou, Zhejiang 310024, China; [c]Department of Chemistry, University of California, Irvine, CA 92697; and [d]Department of Physics and Astronomy, University of California, Irvine, CA 92697

1. S. Mukamel, *Principles of Nonlinear Optical Spectroscopy* (Oxford University Press, 1995).
2. M. Cho, Coherent two-dimensional optical spectroscopy. *Chem. Rev.* **108**, 1331–1418 (2008).
3. C. L. Smallwood, S. T. Cundiff, Multidimensional coherent spectroscopy of semiconductors. *Laser Photon. Rev.* **12**, 1800171 (2018).
4. S. Mukamel *et al*., Roadmap on quantum light spectroscopy. *J. Phys. B: At. Mol. Opt. Phys.* **53**, 072002. (2020).
5. Z. Ficek, P. D. Drummond, Three-level atom in a broadband squeezed vacuum field I. General theory. *Phys. Rev. A* **43**, 6247–6257 (1991).
6. J. Gea-Banacloche, Two-photon absorption of nonclassical light. *Phys. Rev. Lett.* **62**, 1603–1606 (1989).
7. C. W. Gardiner, Inhibition of atomic phase decays by squeezed light: A direct effect of squeezing. *Phys. Rev. Lett.* **56**, 1917–1920 (1986).
8. K. E. Dorfman, F. Schlawin, S. Mukamel, Nonlinear optical signals and spectroscopy with quantum light. *Rev. Mod. Phys.* **88**, 045008. (2016).
9. F. Schlawin, K. E. Dorfman, B. P. Fingerhut, S. Mukamel, Suppression of population transport and control of exciton distributions by entangled photons. *Nat. Commun.* **4**, 1782 (2013).
10. D. I. Lee, T. Goodson, Entangled photon absorption in an organic porphyrin dendrimer. *J. Phys. Chem. B* **110**, 25582–25585 (2006).
11. A. R. Guzman, M. R. Harpham, Ö. Süzer, M. M. Haley, T. G. Goodson, Spatial control of entangled two-photon absorption with organic chromophores. *J. Am. Chem. Soc.* **132**, 7840–7841 (2010).
12. O. Varnavski, B. Pinsky, T. Goodson, Entangled photon excited fluorescence in organic materials: An ultrafast coincidence detector. *J. Phys. Chem. Lett.* **8**, 388–393 (2017).
13. N. Ph Georgiades, E. S. Polzik, K. Edamatsu, H. J. Kimble, A. S. Parkins, Nonclassical excitation for atoms in a squeezed vacuum. *Phys. Rev. Lett.* **75**, 3426–3429 (1995).
14. J. Meinel *et al*., Quantum nonlinear spectroscopy of single nuclear spins. *Nat. Commun.* **13**, 5318 (2022).
15. M. Kira, S. W. Koch, R. P. Smith, A. E. Hunter, S. T. Cundiff, Quantum spectroscopy with Schrödinger-cat states. *Nat. Phys.* **7**, 799–804 (2011).
16. B. P. Fingerhut, S. Mukamel, Resolving the electron transfer kinetics in the bacterial reaction center by pulse polarized 2-D photon echo spectroscopy. *J. Phys. Chem. Lett.* **3**, 1798–1805 (2012).
17. M. G. Raymer, A. H. Marcus, J. R. Widom, D. L. P. Vitullo, Entangled photon-pair two-dimensional fluorescence spectroscopy (EPP-2DFS). *J. Phys. Chem. B* **117**, 15559–15575 (2013).
18. B. Gu, D. Keefer, S. Mukamel, Wave packet control and simulation protocol for entangled two-photon absorption of molecules. *J. Chem. Theory Comput.* (2021).
19. B. Gu *et al*., Photoisomerization transition state manipulation by entangled two-photon absorption. *Proc. Natl. Acad. Sci. U.S.A.* **118**, e2116868118. (2021).
20. B. Gu, S. Mukamel, Manipulating two-photon-absorption of cavity polaritons by entangled light. *J. Phys. Chem. Lett.* **11**, 8177–8182 (2020).
21. D. Tabakaev *et al*., Spatial properties of entangled two-photon absorption. *Phys. Rev. Lett.* **129**, 183601. (2022).
22. J. Javanainen, P. L. Gould, Linear intensity dependence of a two-photon transition rate. *Phys. Rev. A* **41**, 5088–5091 (1990).
23. M. G. Raymer, T. Landes, A. H. Marcus, Entangled Two-Photon Absorption by Atoms and Molecules: A Quantum Optics Tutorial. arXiv [Preprint] (2021). http://arxiv.org/abs/2103.02551 [quant-ph].
24. T. Landes *et al*., Quantifying the enhancement of two-photon absorption due to spectral-temporal entanglement. *Opt. Exp. OE* **29**, 20022–20033 (2021).
25. J. D. Franson, Two-photon interferometry over large distances. *Phys. Rev. A* **44**, 4552–4555 (1991).
26. F. Chen, S. Mukamel, Entangled two-photon absorption with Brownian-oscillator fluctuations. *J. Chem. Phys.* **156**, 074303. (2022).
27. A. Svidzinsky *et al*., Enhancing stimulated Raman excitation and two-photon absorption using entangled states of light. *Phys. Rev. Res.* **3**, 043029. (2021).
28. C. K. Hong, Z. Y. Ou, L. Mandel, Measurement of subpicosecond time intervals between two photons by interference. *Phys. Rev. Lett.* **59**, 2044–2046 (1987).
29. S. Asban, K. E. Dorfman, S. Mukamel, Interferometric spectroscopy with quantum light: Revealing out-of-time-ordering correlators. *J. Chem. Phys.* **154**, 210901. (2021).
30. S. Asban, V. Y. Chernyak, S. Mukamel, Nonlinear quantum interferometric spectroscopy with entangled photon pairs. *J. Chem. Phys.* **156**, 094202. (2022).
31. K. E. Dorfman, S. Asban, B. Gu, S. Mukamel, Hong-Ou-Mandel interferometry and spectroscopy using entangled photons. *Commun. Phys.* **4**, 49 (2021).
32. A. Eshun *et al*., Investigations of molecular optical properties using quantum light and Hong–Ou-mandel interferometry. *J. Am. Chem. Soc.* **143**, 9070–9081 (2021).
33. D. A. Kalashnikov *et al*., Quantum interference in the presence of a resonant medium. *Sci. Rep.* **7**, 11444 (2017).
34. J. Gea-Banacloche, Two-photon absorption of nonclassical light. *Phys. Rev. Lett.* **62**, 1603–1606 (1989).
35. V. Vallet, Z. Lan, S. Mahapatra, A. L. Sobolewski, W. Domcke, Time-dependent quantum wave-packet description of the $1\pi\sigma^*$ photochemistry of pyrrole. *Faraday Discuss.* **127**, 283–293 (2004).
36. G. Wu *et al*., Excited state non-adiabatic dynamics of pyrrole: A time-resolved photoelectron spectroscopy and quantum dynamics study. *J. Chem. Phys.* **142**, 074302. (2015).
37. B. Gu, D. Keefer, S. Mukamel, Wave packet control and simulation protocol for entangled two-photon absorption of molecules. *J. Chem. Theory Comput.* **18**, 406–414 (2022).
38. S. Mukamel, Partially-time-ordered Schwinger-Keldysh loop expansion of coherent nonlinear optical susceptibilities. *Phys. Rev. A* **77**, 023801. (2008).
39. T. E. Keller, M. H. Rubin, Theory of two-photon entanglement for spontaneous parametric down-conversion driven by a narrow pump pulse. *Phys. Rev. A* **56**, 1534–1541 (1997).
40. M. H. Rubin, D. N. Klyshko, Y. H. Shih, A. V. Sergienko, Theory of two-photon entanglement in type-II optical parametric down-conversion. *Phys. Rev. A* **50**, 5122–5133 (1994).
41. W. J. Glover *et al*., Excited state non-adiabatic dynamics of the smallest polyene, trans 1,3-butadiene. II. Ab initio multiple spawning simulations. *J. Chem. Phys.* **148**, 164303 (2018).
42. S. Sun, D. B. Williams-Young, T. F. Stetina, X. Li, Generalized Hartree-Fock with nonperturbative treatment of strong magnetic fields: Application to molecular spin phase transitions. *J. Chem. Theory Comput.* **15**, 348–356 (2019).
43. D. T. Colbert, W. H. Miller, A novel discrete variable representation for quantum mechanical reactive scattering via the S -matrix Kohn method. *J. Chem. Phys.* **96**, 1982–1991 (1992).
44. R. Kosloff, Time-dependent quantum-mechanical methods for molecular dynamics. *J. Chem. Phys.* **92**, 2087–2100 (1988).